Stochastic orbit loss of neutral beam ions from NSTX due to toroidal Alfvén eigenmode avalanches

D.S. Darrow[1], N. Crocker[2], E.D. Fredrickson[1], N.N. Gorelenkov[1], M. Gorelenkova[1], S. Kubota[2], S.S. Medley[1], M. Podestà[1], L. Shi[1] and R.B. White[1]

[1] Princeton Plasma Physics Laboratory, Princeton, NJ 08543-0451, USA
[2] Department of Physics, University of California, Los Angeles, CA, USA

E-mail: ddarrow@pppl.gov

Abstract
Short toroidal Alfvén eigenmode (TAE) avalanche bursts in the National Spherical Torus Experiment (NSTX) cause a drop in the neutron rate and sometimes a loss of neutral beam ions at or near the full injection energy over an extended range of pitch angles. The simultaneous loss of wide ranges of pitch angle suggests stochastic transport of the beam ions occurs. When beam ion orbits are followed with a guiding centre code that incorporates the plasma's magnetic equilibrium plus the measured modes, the predicted ranges of lost pitch angle are similar to those seen in the experiment, with distinct populations of trapped and passing orbits lost. These correspond to domains where the stochasticity extends in the orbit phase space from the region of beam ion deposition to the loss boundary and the trajectories along which modes may transport particles extend from the deposition volume to the loss boundary.

1. Introduction

In National Spherical Torus Experiment (NSTX) [1–3] plasmas, short ($\leqslant 2$ ms) bursts of toroidal Alfvén eigenmodes (TAEs) [4, 5] are sometimes seen with multiple toroidal mode numbers, n, present simultaneously. These are termed TAE avalanches [6]. These avalanches are always accompanied by drops in the neutron rate of the order of 5–25%. Neutron production in NSTX results predominantly from reactions of the injected 90 keV deuterons with bulk plasma deuterons, which typically have a temperature in the range of 1–2 keV. Because the avalanches do not usually change the bulk plasma profiles appreciably, the drops in neutron rate have been attributed to neutral beam ion redistribution or loss. NSTX is equipped with a gyroradius and pitch angle dispersing scintillator-type fast ion loss diagnostic [7] capable of measuring any associated loss. Interestingly, this diagnostic shows fast ion loss for some but not all avalanches. In addition, when losses are seen, the pitch angle range of the lost particles can vary substantially. In this work, we compare avalanches in two similar discharges in NSTX, one that evidences loss on the scintillator detector and one that does not. In concert with this, we recently applied a developed phase space mapping technique [8] that can identify which portions of the particle

orbit phase space are stochastic given an equilibrium, mode structures, and mode amplitudes. This technique predicts little loss to the detector in the avalanche where no losses are detected, while it predicts losses over pitch angle ranges that are similar to those measured in the case with loss. A similar rapid loss of ICRF heated tail ions in the ASDEX-Upgrade tokamak occurs when multiple Alfvénic modes are present [9], and these have similarly been understood by consideration of resonance overlaps in phase space [10]. Loss of neutral beam ions over an extended range of pitch angles due to bursting MHD has also been reported from the Compact Helical System (CHS) [11].

2. Observed avalanche characteristics

Characteristics are presented here for avalanches in two similar NSTX L-mode discharges. L-mode discharges were chosen for this study as the more gradual density gradient from the edge to plasma centre (compared to H-mode plasmas) allows a microwave reflectometer system (discussed below) to obtain mode amplitude data over a wide range of positions within the plasma. Figure 1 shows the time histories of two nearby discharges with similar parameters. Marked in the figure are
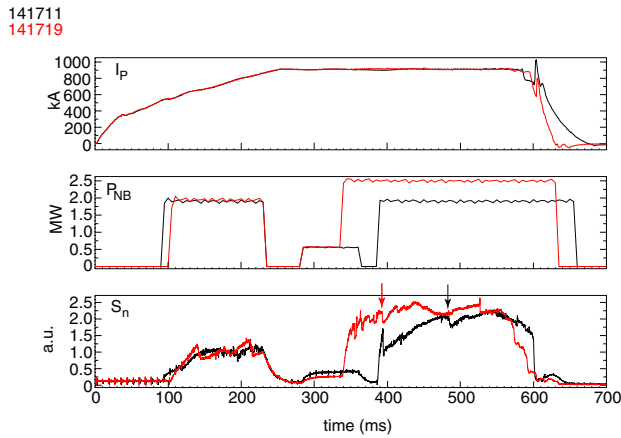
Figure 1. Time histories of the plasma current, neutral beam heating power, and neutron rate in two NSTX plasmas where TAE avalanches occur. The shots have similar conditions. In shot 141711, there is a TAE avalanche at 483 ms in which the fast ion loss detector sees no neutral beam ion loss. In shot 141719, there is an avalanche at 393 ms during which fast ion losses are observed. In both cases, the neutron rate drops by 17%.

times at which TAE avalanches occur, causing a reduction in the neutron rate. Both avalanches have several n numbers (toroidal mode numbers) simultaneously present. But, for the case plotted in black (shot 141711), there is no loss observed by the scintillator loss probe. This discharge has a single 90 kV neutral beam injecting at the time of interest (483 ms). Contrastingly, in the case plotted in red (shot 141719), there is an avalanche in which losses are observed. In this discharge, a second neutral beam source, operating at 60 kV, has been added to the original source injecting at 90 kV. This presumably increases the drive of the TAEs relative to the case with only a single beam injecting. In both plasmas, the avalanches studied reduce the neutron rate by 17%, making them seemingly equal from this gross measure of the effect on fast ions.

Global mode characteristics are presented below for the avalanches with and without observed fast ion loss. Figure 2 shows the frequency spectrogram of a Mirnov coil over the course of the avalanche exhibiting no loss, along with the rms amplitude of the Mirnov coil signal, and the neutron rate. Toroidal mode numbers 1 through 5 are seen to be present, first as weakly bursting modes, then appearing all together in an avalanche after 483 ms. A comparable set of plots for the avalanche exhibiting detectable loss is shown in figure 3.

Toroidal mode numbers 2, 3 and 4 are present in this shot at amplitudes comparable to or lower than those in the no-loss shot. Included in this plot is the total detected loss flux as a function of time. This plot has been constructed by summing the total observed intensity in the scintillator probe camera frames over the time period of interest. The camera for these discharges was acquiring images at 30 000 frames s^{-1}, giving a 33 μs time resolution. Note that the peak loss flux occurs slightly after the time of peak magnetic amplitude in this avalanche, just after all the modes individually have reached their peak amplitudes. The units for rms magnetic fluctuation and neutron rate, though uncalibrated, are the same in both figures. Note also that there is no loss observed before and after the avalanche, indicating that prompt orbit losses are tiny and not seen by the detector in this condition.
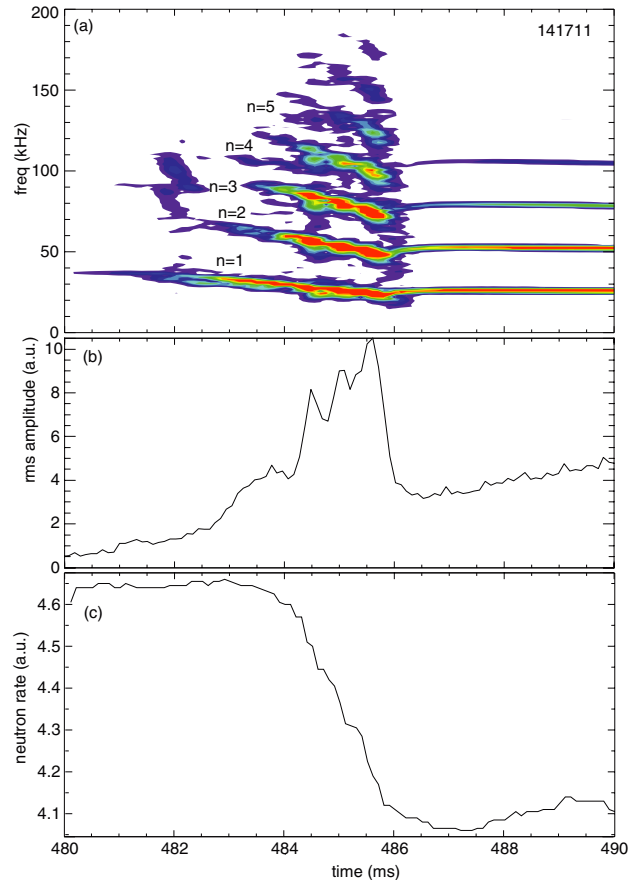

Figure 2. (*a*) Frequency spectrogram of a magnetic pickup coil signal in the avalanche with no beam ion loss observed. Toroidal mode numbers $n = 1, 2, 3, 4$, and 5 are present, as determined by a toroidal array of pickup coils. The rms magnetic fluctuation amplitude (*b*) and neutron rates (*c*) versus time are also shown. The neutron rate drops by 17% as a result of the avalanche.

Figure 4 shows the four camera frames that have measurable loss for the avalanche in 141719. All frames before and after these four show no loss at all. In the first two frames, a small spot can be seen on the right, which is consistent with the loss of full beam energy particles that have predominantly perpendicular velocities. This loss persists into the third and fourth frames, but is supplemented by loss over a range of more parallel-going pitch particles. After the fourth frame, the loss event has completely concluded. Figure 5 shows the brightest of the frames with loss (the third) with a superimposed interpretation grid for the gyroradius and pitch angle of the lost particles. From this figure, it can be seen that the rightmost loss spot covers a range in pitch angle from 56° to 65°, all corresponding to trapped particle orbits. Here, the pitch angle is defined as $\chi = \arccos(v_{\parallel}/v_{\text{tot}})$. The left spot extends from 18° to 40° pitch angle, and orbits over that entire range of pitch angles are passing.

In addition to the direct measurements of beam ion loss from the scintillator probe, loss can also be inferred from the signal of a charge exchange energetic neutral particle analyser (NPA) [13]. Figure 6 displays the time traces of a channel that detects 90 keV D neutrals emanating from the plasma during the avalanches under investigation. For this measurement, the NPA sight line was on the midplane, at a
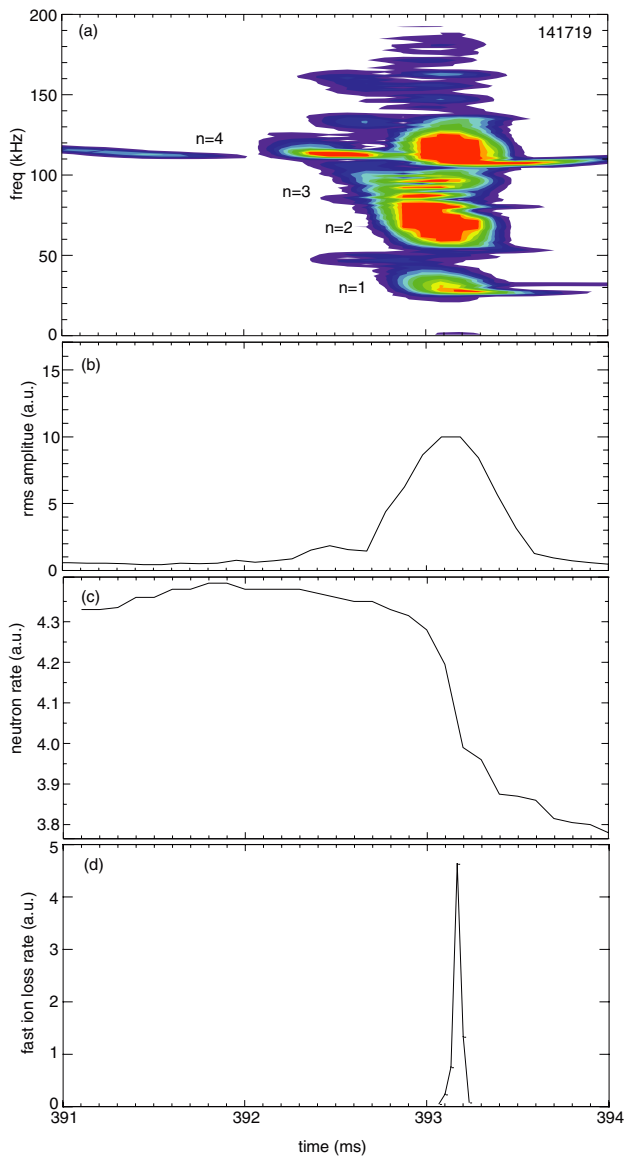
Figure 3. (*a*) Magnetic pickup coil frequency spectrogram during avalanche on an expanded time scale, (*b*) total magnetic fluctuation amplitude, (*c*) neutron rate, and (*d*) total fast ion loss rate measured by the detector, all as functions of time during the avalanche in shot 141719, which does exhibit measurable losses. The detector loss rate is the summed brightness in each camera image taken over the course of the event (33 μs per frame) minus any black level.

Figure 4. Sequence of fast ion loss detector camera frames in shot 141719 over the duration of the avalanche. Each frame covers 33 μs. All frames before and after the sequence shown are black, indicating no loss to the detector at those times. Details of the pitch angle and gyroradius of the lost ions are in figure 5.

3. Modelling of particle loss and the stochastic domains

In order to better understand and characterize the processes affecting the beam ion loss, we analysed the guiding centre orbits of full energy D beam ions in the magnetic equilibria at the times of interest and including the influence of the fields of the TAEs present in each avalanche. This was done with the ORBIT code [8, 12]. The plasma magnetic equilibria used in this modelling were produced by EFIT [14] or LRDFIT [15] at or near the times of interest. The fields

tangency radius of 0.70 m. The 90 kV beam in this plasma was injecting at a tangency radius of 0.60 m, close to the radius measured by the NPA. This internal measurement of the 90 keV D ion density corroborates the loss measurements. For 141711 where essentially no loss is seen there is no significant change to the NPA flux over the course of the avalanche. Contrast this to the event in shot 141719 with clear losses. The NPA trace in this case shows a distinct drop in the energetic ion density during this avalanche, again consistent with the loss measurements. In 141719, NPA energy channels down to ~50 keV also show a drop in flux at the time of avalanche. This drop in flux persists over approximately a slowing down time, with the flux at lower energies taking longer to return to its pre-avalanche levels than the flux at higher energies.
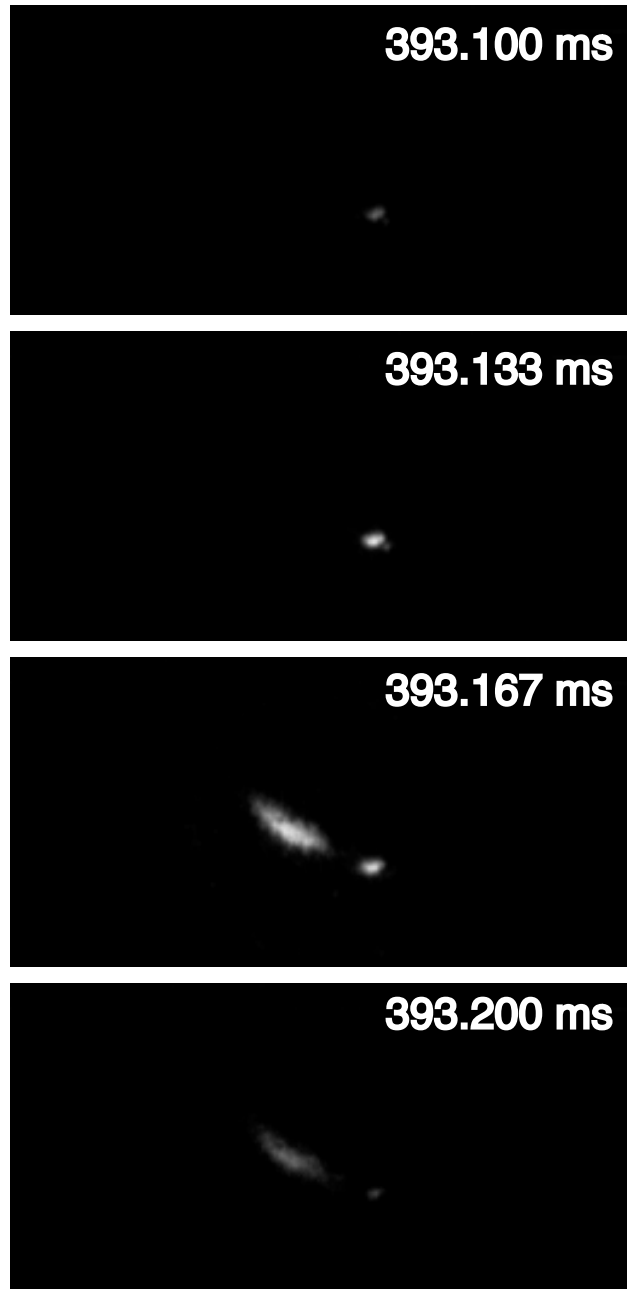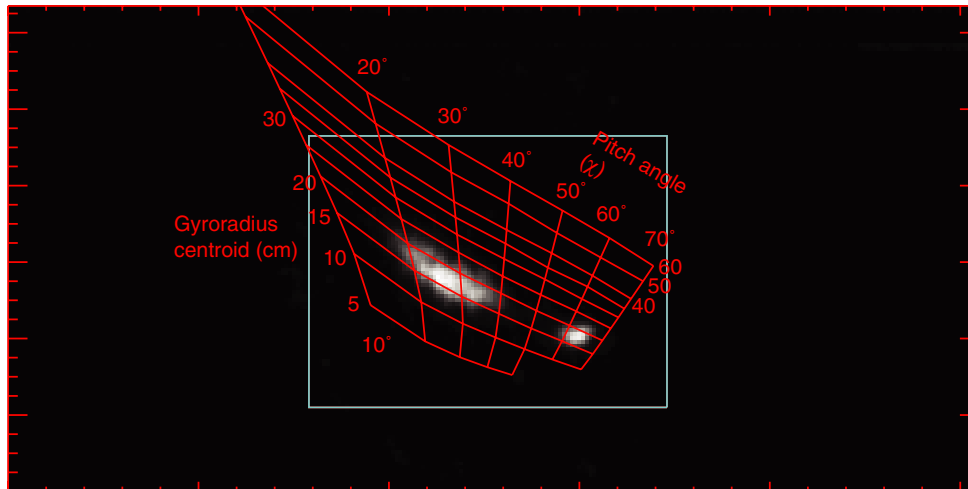
Figure 5. Camera frame at time of peak loss (393.167 ms) with interpretive grid defining the gyroradius centroid and pitch angle of the lost particles. The pitch angle is defined to be $\chi = \arccos(v_{\parallel}/v_{\text{tot}})$ and the gyroradius centroid is v_{tot}/Ω_i. The latter definition means that the gyroradius centroid is a function of the particle's total energy only, irrespective of the proportions of parallel and perpendicular velocity. The superimposed rectangle depicts the extent of the scintillator plate within the diagnostic. Based upon the EFIT magnetic field at the detector location, 90 keV D ions should have a gyroradius of 17 cm. This is consistent with the observed loss displayed here and validating the focus of modelling the behaviour of recently injected (i.e. not substantially slowed down) beam ions.

of the TAEs were modelled in the following way: first, the discharge was modelled with the TRANSP [16] transport code in order to obtain a consistent set of radial profiles of plasma parameters in the equilibrium at the time of interest. Where possible, the directly measured profiles were used for fitting of the mode structures. The equilibrium and profile data, along with the n numbers observed by an array of Mirnov coils, were used as input to the NOVA-K code [2] to compute the TAE structures at the time of the avalanche. Since the NOVA-K code only computes the eigenmode structure with an arbitrary amplitude, the final step was to take plasma surface displacement measurements at each mode frequency as measured by a 16 channel microwave reflectometer system [17] and scale the NOVA-K eigenmodes to an overall amplitude that produced the best fit to the measured displacements. This process then provides absolute amplitudes for the modes at all points within the plasma. The fitted modes are represented as a set of coefficients, α, such that the mode fields are given by $\delta \boldsymbol{B} = \nabla \times (\alpha \boldsymbol{B})$. Because the fitted radial amplitude profiles can have spikes and other numerical artefacts that adversely affect subsequent orbit computations, some radial smoothing was applied to the fitted eigenfunctions, and the amplitudes were set to zero at points of intersection of the eigenfunction with the Alfvén continuum. This is the same process previously applied for modelling the drop of the neutron rate in NSTX during avalanches [6]. For the cases studied, poloidal Fourier harmonics up to $m = 15$ were retained to provide a good fit to the measurements. ORBIT includes the E fields of the modes while constraining $E_{\parallel}$ to be zero.

Note that the guiding centre formalism assumes that the magnetic moment ($\mu = mv_{\perp}^2/2B$) is a good conserved quantity for particle motion. This assumption holds if the observed TAE frequencies are well below the ion cyclotron frequency range in NSTX and if the gyroradius of the beam ions is small compared to the wavelength of the modes and the magnetic field gradient scale length of the underlying

equilibrium. The condition on mode frequencies is certainly satisfied in NSTX, where the beam ion cyclotron frequency is $\sim$3 MHz and the modes are of the order of 100 kHz. Similarly, a unique property of spherical tokamak plasmas is that the total magnetic field strength varies only slightly in going from the magnetic axis to plasma edge, producing a long scale length for changes in $|B|$. Hence the constraint on the gradient scale length of the underlying equilibrium is satisfied. With regard to the modes themselves, the strongest constraint is that given by the highest m component retained, namely 15. The reflectometer measurements reveal the mode amplitudes peak at a minor radius of 30 cm. The flux surface there can be approximated as an ellipse with a vertical elongation of 1.5. Thus, the poloidal wavelength of the highest m component used is 19 cm. The particles with the largest gyroradius observed by the loss detector are those with a pitch angle of $\sim$60°. These have a gyroradius of 15 cm. This is smaller than the shortest poloidal wavelength used, though not grossly so. This pitch angle then represents the limit at which guiding centre orbit following may still apply. However, for more passing particles, which will have smaller gyoradii, the method should still be valid. It should be noted that a separate comparison of guiding centre and full gyro-orbit motion for a case with an island a gyroradius wide still showed good agreement between the guiding centre and full orbit calculations.

Given the framework just described, the ORBIT code was able to provide two types of computational results to aid in understanding the observed losses. The first type of calculation was simply to follow the guiding centre orbits of a large number of full energy (90 keV) D neutral beam ions and tabulate characteristics of the ones that were lost. The second calculation was to use the capability of the ORBIT code to evaluate domains in which the orbits can diffuse stochastically under the influence of the TAEs present. These domains could then be compared with regions where beam ions are deposited and lost to ascertain whether stochastic transport might have been responsible for the losses observed. For both types of
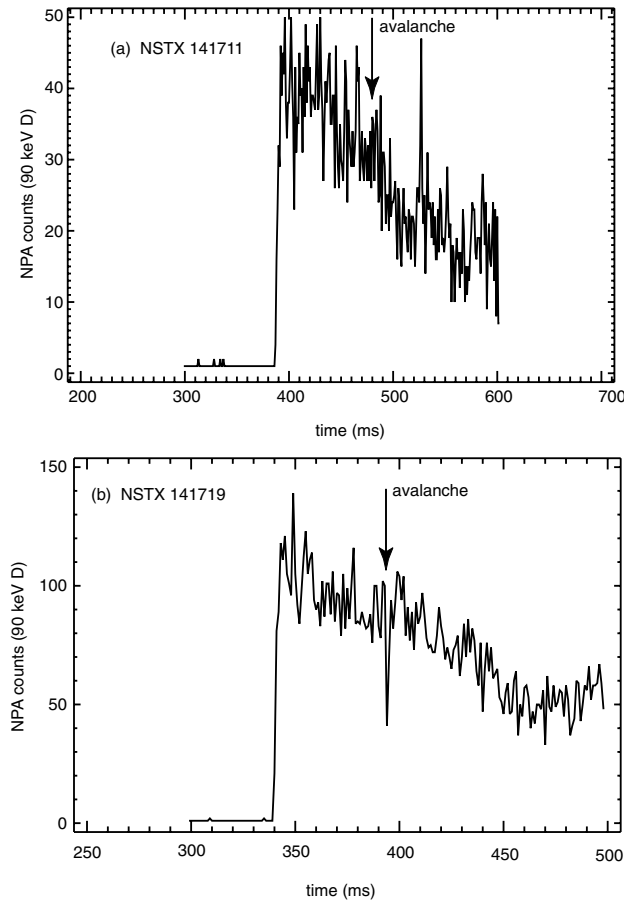
Figure 6. Measurements of the energetic neutral particle flux from the plasma at 90 keV for (*a*) the discharge with an avalanche producing no observable loss and (*b*) the case with a signal seen in the scintillator probe. The times of the avalanches in both discharges are marked. These internal measurements corroborate the external measurement of fast ion loss during the avalanches.

Figure 7. Lost beam ions in the $(E, \mu B_0)$ plane, irrespective of P_ϕ after 2 ms of motion through the avalanche field perturbations in shot 141711. Points in black are all guiding centres that reach the last closed surface. Points in red are lost particles whose orbital parameters (E, μ, P_ϕ) lie within the range of values accepted by the scintillator loss detector. The red diagonal line is the passing/trapped boundary. Particles below this line are passing, while those above it are on trapped orbits. Note that while the loss detector receives particles representative of groups of lost particles at both low and high μB_0, the losses are quite sparse in comparison with the other avalanche considered (figure 8), in concert with the experimental observations.

orbit assessments, the initial population of neutral beam ions was taken to be a random sample of 90 keV D beam ions from the beam deposition calculation performed by TRANSP. Attention was focused solely on these ions because the loss detector sees ions whose gyroradius equals that of 90 keV D ions given the magnetic field strength at the detector. The detector is capable of sensing lower energy losses as well, but none are seen. This observation, and the fact that the avalanche duration is considerably less than a slowing down time (~30 ms) make this choice of focusing only on newly injected full energy ions plausible.

For the first type of calculation mentioned above, orbits were followed for the equivalent of 2 ms in the experiment, and statistics of any particles that were lost were accumulated. In this calculation, a particle was taken to be lost if its guiding centre reached the last closed flux surface. A simulation of the population of particles reaching the scintillator probe was created by taking a subset of the lost particles whose energy, magnetic moment, and canonical toroidal momentum were within the range that could be received by the detector. Starting beam ion guiding centre populations were taken from TRANSP simulations of the discharges in question, at the times of interest, and those populations were restricted to freshly deposited full energy beam ions.
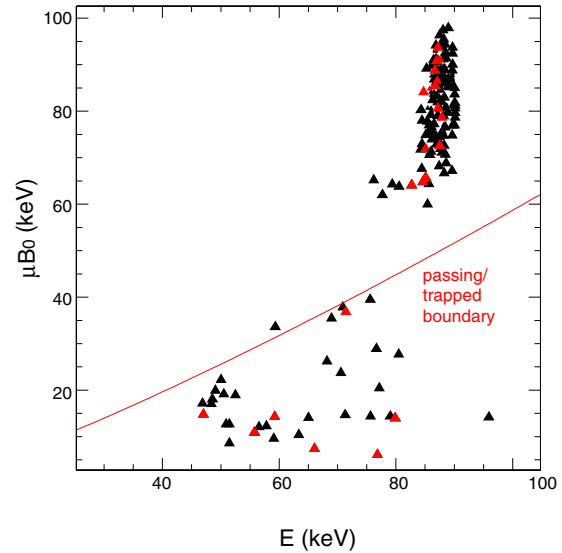
Figure 7 shows the accumulated populations of lost particles, in the $(E, \mu B_0)$ plane, where B_0 is the field strength at the magnetic axis. μB_0 is essentially a measure of a particle's pitch angle, but has units of energy. Particles are shown at all values of P_ϕ. The plot shows losses both anywhere at the last closed surface and also restricted to those orbits that are able to reach the detector for the avalanche in 141711 (case of no observed loss). Particles in this simulation are counted as having reached the detector if their E, μ and P_ϕ fall within the range of those values defined by the actual aperture acceptance at the detector's real location. Note that such particles might not actually reach the detector since this criterion sets no restriction on the particle's toroidal angle. This method does, however, provide a simple calculation of the possible loss flux to the detector.

The calculation shown in figure 7 was performed with an initial population of 100 000 beam ions. Only a few lost particles appear within the acceptance of the detector, consistent with the observation in this case. Interestingly, though, a few particles were found in this simulation whose interactions with the modes caused them to slow down rapidly (to 30 keV in 5 ms in one slightly extended simulation) while still remaining confined. Since the DD neutron cross section decreases very rapidly with decreasing energy, it is possible behaviour of this sort could explain some portion of the drop in neutron rate observed. It is a potential topic for future study to investigate what fraction of particles exhibit this type of interaction with the modes, and whether there are any unique characteristics of the modes that promote continued confinement of particles coupled with rapid slowing down
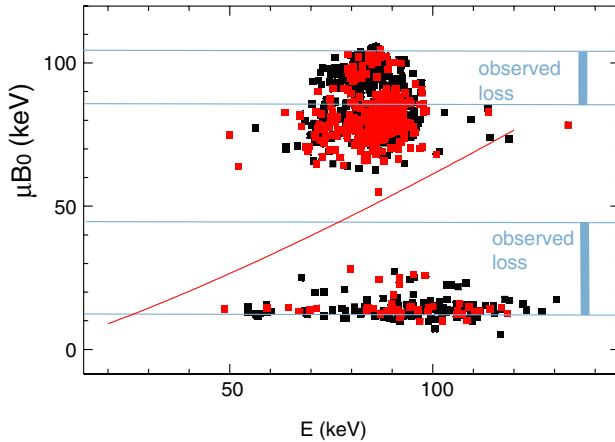
5

Figure 8. Lost beam ions in the $(E, \mu B_0)$ plane, irrespective of P_ϕ after 2 ms of motion through the avalanche field perturbations in shot 141719, starting with 1 000 000 initial beam particles. Points in black are all guiding centres that reach the last closed surface. Points in red are lost particles whose orbital parameters (E, μ, P_ϕ) lie within the range of values accepted by the scintillator loss detector. Losses seen by the detector in this case again are representative of the groups of particles lost (as in figure 7). Also marked on this plot in blue are the extents of the two loss spots seen in the detector image in figure 5. The solid curve is the passing/trapped boundary.

Figure 9. Modelled and measured loss flux as a function of μB_0. The fluxes are integrated over all E and P_ϕ. The black (short dashed) and red (long dashed) curves are, respectively, guiding centres that cross the last closed flux surface and guiding centres whose orbital parameters are within the range of acceptance of the detector apertures. For these two curves, the flux units are in particles per interval in μB_0, out of an initial population of 100 000. The blue (solid) curve is the measurement (figure 5) mapped onto units of μB_0 for the horizontal axis and arbitrary units on the vertical axis.

rather than outright loss of the particles. A global loss fraction of 0.75% was calculated in this case. The loss fraction in the absence of the modes (i.e. prompt loss) is computed to be much smaller than this. When the orbit-following process was repeated for shot 141719, where losses were actually observed, the orbit-following code did find more losses occurring, especially at the detector. A total loss fraction of 2% was computed, significantly larger than the loss in shot 141711. Figure 8 shows a plot of the lost particles in the $(E, \mu B_0)$ plane for this case. This calculation shows a bimodal loss distribution with two discrete bunches of particles lost over different ranges of μB_0 (which translates to two ranges in pitch angle). This bears resemblance to the loss detector measurement, which also has two discrete groups of lost particles. For purposes of comparison, the ranges over which the detector finds losses are also marked. There is good agreement on the boundaries of the loss at the highest and lowest values of μB_0, but the agreement is not as good at the intermediate boundaries. The reason for this is not understood.

The differences between the modelled and measured loss distributions are more clearly visible in figure 9, which portrays the total lost ion flux as a function of μB_0 (i.e. pitch angle) integrated over all energies and all values of P_ϕ for both the orbit modelling and the measurement. (Note that values of μB_0 that exceed the particle energy are indicative of deeply trapped particles on orbits which never reach a position where $|B|$ approaches B_0). Over the range in μB_0 between 30 and 60 keV, the orbit modelling predicts essentially zero loss, while the experiment displays clear loss throughout the range. In contrast, between 65 and 85 keV, the measured loss is minimal, while the modelled loss is at its peak.

Further simulations were performed with additional components to see if the model results would come to a closer agreement with the measurements. Items tried included a larger population of particles for better statistics, inclusion
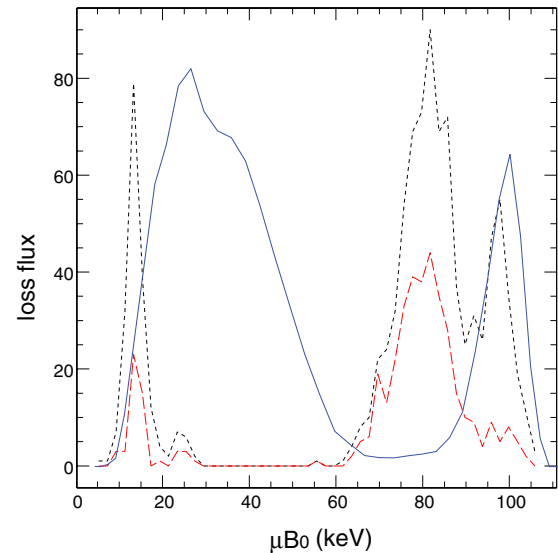
of the radial electric field profile, and inclusion of the time evolution of the mode frequencies and amplitudes over the course of the burst. None of these phenomena changed the calculation result greatly. It is worth noting that the lack of substantial change of the loss characteristics when the mode frequency was varied also supports attributing these losses to stochastic phenomena. Loss due to resonant interaction of particles with the modes ought to have changed significantly as the mode frequencies were varied in the simulation, but this was not seen. Having exhausted the possibilities noted above as possible reasons for disagreement between the measured and modelled lost particle pitch angle profile, we suspect that this is related to uncertainties in or approximations used in the fitting of the TAE mode structures to the reflectometer measurements, as described previously.

The observation that particles are lost over a range of pitch angles in this avalanche suggests that the process of particle loss does not proceed by way of individual isolated resonant interactions between the modes and particles. In that case, localized spots in pitch angle would seem most likely, corresponding to orbits whose transit or bounce frequencies resonate with one of the modes within the avalanche. Instead, the observed signature seems more characteristic of loss resulting from stochastization of the particle orbit phase space by the presence of multiple TAEs. The wave–particle resonances are present, of course, as evidenced by the fact the modes are driven unstable. The loss arises due to the simultaneous existence of several modes that have reached an amplitude large enough to produce phase space stochastization. In order to investigate the hypothesis that portions of the orbit phase space have become stochastic, the ORBIT code was run in a mode where stochastic domains of the particle orbit
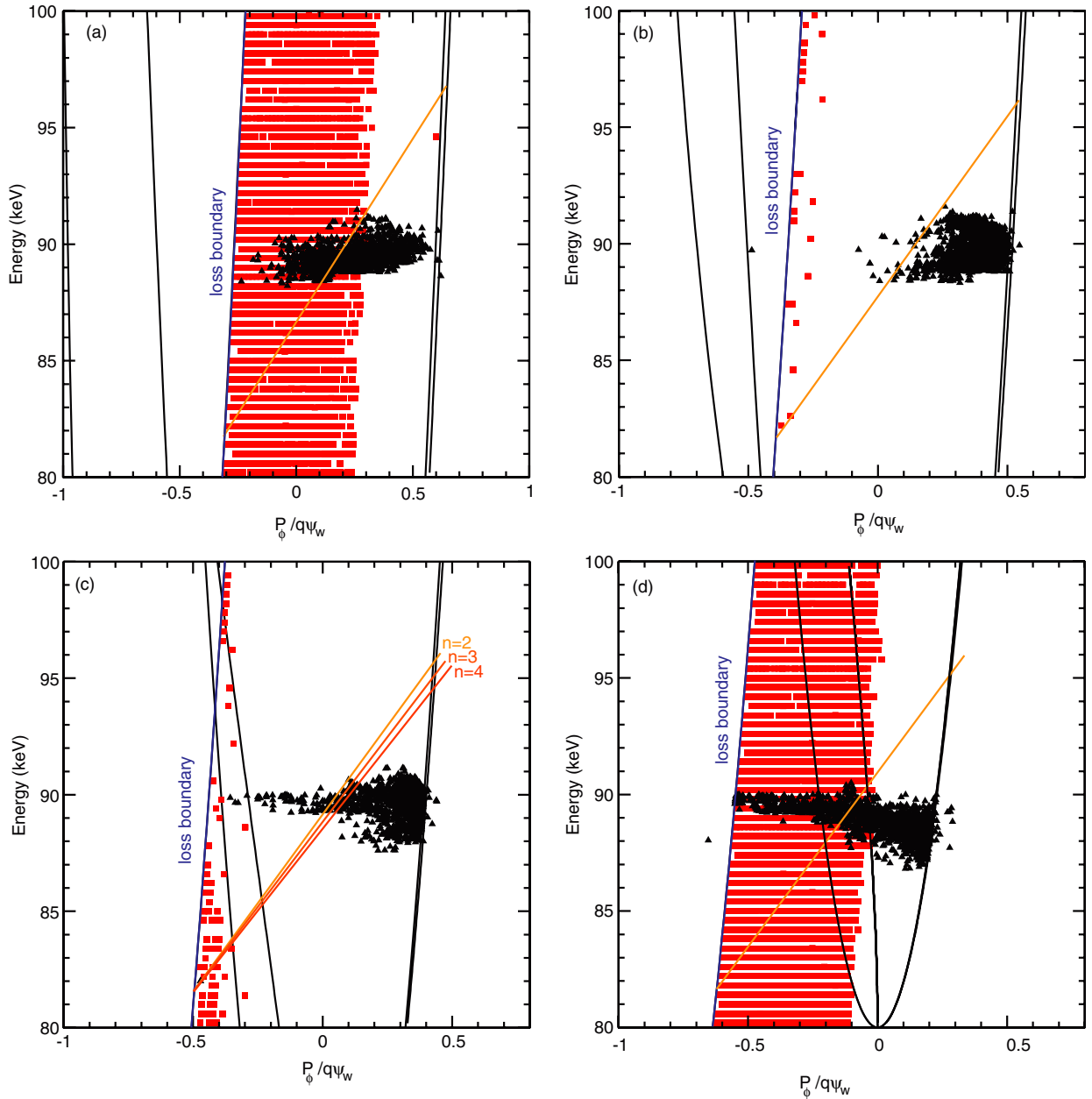
Figure 10. Maps of the stochastic domains in the (E, P_ϕ) plane for four values of μB_0 in shot 141719. (*a*) $\mu B_0 = 20$ keV (23° pitch angle at scintillator detector), (*b*) $\mu B_0 = 40$ keV (33° pitch angle at the scintillator detector), (*c*) $\mu B_0 = 60$ keV (43° pitch angle at the scintillator detector), and (*d*) $\mu B_0 = 80$ keV (52° pitch angle at the scintillator detector). In each plot, the following entities are represented: (1) Black triangles are deposited neutral beam ions. (2) Red squares are points in the orbit phase space where stochasticity is found using the methodology described in the text. (3) The blue curve to the left of each panel is the orbit code's confinement boundary, namely where guiding centres reach the last closed flux surface. (4) The leftmost and rightmost black curves delineate guiding centres on the magnetic axis, and the intermediate black curve is the passing/trapped boundary. (5) An orange line indicating the direction in which particles would move diffusively under the influence of the $n = 2$ TAE in the avalanche. Particles can move along any line of the same slope in the frame shown. Plot (*c*) includes lines for $n = 2$, 3 and 4, showing that the direction of diffusion under the influence of any of these modes is substantially similar. From these plots, it is evident that stochastic transport of deposited beam ions to the loss boundary can occur for the μB_0 values (pitch angles) depicted in (*a*) and (*d*). This is broadly consistent with pitch angles at which loss is seen in the experiment, at least in the sense that a passing and trapped population of particles are subject to this loss process. In cases (*b*) and (*c*), beam ions are deposited in regions of good surfaces and are hence not subject to any stochastic transport.

phase space could be mapped. This method is described in detail in [8], but consists in essence of following a pair of nearby guiding centres over a series of toroidal transits. A 'phase vector' in the (θ, P_ϕ) plane (where θ is the position of the guiding centre in poloidal angle and $P_\phi = m v_\phi R - q\psi$ is the canonical toroidal momentum of the guiding centre) is

constructed between the two guiding centres at the completion of each transit, and its orientation angle ('phase angle') in the plane recorded. If good drift orbit surfaces exist in the particle phase space, then this phase angle cannot vary by more than π radians. If the phase angle varies by greater than that amount, the local region where the orbits have been started must be

stochastic. This process can then be repeated for closely spaced pairs of particles anywhere in the space.

As noted above, the magnetic moment of a particle is conserved while it interacts with the TAEs in the avalanche, although the energy and canonical toroidal momentum can vary. For interaction of a particle with a single mode, the particle would be constrained to move along a line $nE - \omega P_\phi =$ constant in the (E, P_ϕ) plane.

Due to the presence of multiple TAEs, the Kolmogorov–Arnold–Moser (KAM) surfaces in the beam ion phase space may be broken. In this circumstance, there exists an Arnold web, consisting of lines in the (E, P_ϕ) plane. (In many systems, the Arnold web is comprised of an intricate spider web arrangement crisscrossing the plane, hence the appellation 'web'.) Arnold diffusion is diffusion along a resonance line in the Arnold web. Normally it is not very rapid. Because the lines $nE - \omega P_\phi =$ constant are in all cases observed far from parallel to the lines of resonance in the Arnold web, Arnold diffusion cannot be produced by a single mode. However, if modes of different frequency have resonances in the same region of the (E, P_ϕ) plane, the motion due to the two modes can combine to produce diffusion along the resonance surface, giving Arnold diffusion. Shown in figure 10 are cases observed in the simulation of loss from shot 141719, including the resonant domains and the slope of the lines along which orbits move for each mode. Each mode produces a broad resonant region, consisting of more than one almost vertically aligned island chain, close to the plasma boundary.

In the (E, P_ϕ) plane at constant μ it is also possible to define the loss boundary for particles. In the ORBIT code, this boundary is defined as the guiding centre reaching the last closed flux surface, although it is possible to apply finite Larmor radius corrections. Furthermore, for a given value of μ, TRANSP-deposited full energy beam ions whose μ lies within a small range above or below the chosen value can also be plotted as individual points in the (E, P_ϕ) plane. The resultant plots containing the deposited particle population, the loss boundary, the lines of motion for each mode, and the stochastic domain are shown in figure 10 for several values of μB_0. Plots such as those in this figure are then capable of revealing values of μ at which stochastic losses are possible. For stochastic loss of particles to occur at a given value of μ, the following things must be true: first, the particles are born in a stochastic region of the orbit phase space. Second, a line of the form $nE - \omega P_\phi =$ constant must extend from the position of particle deposition to the loss boundary. Third, the orbit phase space must be stochastic at every point along that line between the birth position and the loss boundary. Figure 10 shows examples of when stochastic loss is expected ((a) $\mu B_0 = 20$ keV and (d) $\mu B_0 = 80$ keV), and when stochastic loss should not arise ((b) $\mu B_0 = 40$ keV and (c) $\mu B_0 = 60$ keV).

These plots do reveal that there are two domains in the fast ion phase space subject to stochastic transport, one passing and one trapped. This is consistent with the measurement.

As noted above, the highest and lowest pitch angle boundaries (i.e. boundaries in μB_0) agree with those observed, though the interior pitch angle boundaries (namely the high pitch angle or high μB_0 boundary of passing particle loss and the low pitch angle or low μB_0 limit of trapped particle loss) do not agree so well.

4. Conclusions

TAE avalanches in NSTX exhibit fast ion loss signatures including no observed loss or loss over multiple ranges of pitch angle. Guiding centre orbit modelling of the full energy deposited beam ion population including the effects of the TAEs at their measured amplitudes reproduce the character of the loss and some elements of the pitch angle range of the loss. The loss in the case most closely studied here appears consistent with stochastization of the particle orbit space by the modes. The stochastization can produce losses when it extends contiguously in particle phase space from the region of beam ion deposition to the plasma boundary along a line defined by $nE - \omega P_\phi =$ constant. This study indicates that matching the measured pitch angle distribution of the loss at a detector provides a substantial additional challenge against which to test numerical simulations of fast ion transport in multi-mode events such as avalanches.

References

[1] Spitzer J. *et al* 1996 *Fusion Technol.* **30** 1337
[2] Ono M. *et al* 2001 *Nucl. Fusion* **41** 1435
[3] Peng Y.-K.M. and Strickler D.J. 1986 *Nucl. Fusion* **26** 769
[4] Cheng C.Z. and Chance M.S. 1986 *Phys. Fluids* **29** 3695
[5] Heidbrink W.W. 2008 *Phys. Plasmas* **25** 055501
[6] Fredrickson E.D. *et al* 2009 *Phys. Plasmas* **16** 122505
[7] Darrow D.S. 2008 *Rev. Sci. Instrum.* **79** 023502
[8] White R.B. 2012 *Commun. Nonlinear Sci. Numer. Simul.* **17** 2200
[9] García-Muñoz M. *et al* and the ASDEX Upgrade Team 2010 *Phys. Rev. Lett.* **104** 185002
[10] García-Muñoz M. *et al* and the ASDEX Upgrade Team 2010 *Nucl. Fusion* **50** 084004
[11] Shinohara K., Isobe M., Darrow D.S., Shimizu A., Nagaoka K. and Okamura S. 2007 *Plasma Fusion Res.* **2** 042
[12] White R.B. and Chance M.S. 1984 *Phys. Fluids* **27** 2455
[13] Medley S.S. and Roquemore A.L. 2004 *Rev. Sci. Instrum.* **75** 3625
[14] Lao L. *et al* 1985 *Nucl. Fusion* **25** 1611
[15] Levinton F.M. *et al* 2007 *Phys. Plasmas* **14** 056119
[16] Hawryluk R.J. 1980 *Physics of Plasmas Close to Thermonuclear Conditions* vol 1, ed B. Coppi *et al* (Brussels: CEC) p 19
[17] Crocker N. *et al* 2011 *Plasma Phys. Control. Fusion* **15** 105001